Computers and Electronics in Agriculture 209 (2023) 107848

Contents lists available at ScienceDirect

Computers and Electronics in Agriculture

journal homepage: www.elsevier.com/locate/compag

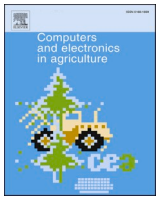

Assessing the influence of crop model structure on the performance of data assimilation for sugarcane

Izael M. Fattori Jr. *, Fábio R. Marin

University of São Paulo (USP), College of Agriculture "Luiz de Queiroz" (Esalq), Piracicaba, SP, Brazil

ARTICLE INFO

Keywords:
Ensemble Kalman filter
DSSAT/SAMUCA
WOFOST
Landsat
Remote sensing
Leaf area index

ABSTRACT

Process-base crop models (PBM) are important tools to describe how the agricultural system responds to environmental conditions. Sugarcane represents a major world source of sugar and ethanol and its PBMs had different levels of complexity in terms of structure, i.e. how detailed their processes were described. Yet, literature has widely demonstrated that data assimilation techniques (DA) represent a valuable option for reducing model uncertainty, but the inconsistency between PBM and the assimilated variable can significantly affect the performance of DA. Such limitation is strictly connected to model structure, and a hypothesis that arises from literature is that the use of more complex models would reduce model uncertainty after DA. We accessed the performance of using two different PBMs, one more detailed (DSSAT/SAMUCA, DS) and the other more general (WOFOST, WO), by assimilating leaf area index (LAI) retrieved from Landsat 7 ETM + and 8/OLI, using the Ensemble Kalman Filter (EnKF). Both PBMs were calibrated and evaluated with a robust database of 13 experiments and evaluated against a sugarmill database to evaluate the EnKF performance, compared with simulations without DA (Open-loop, OP). Moreover, the processes involved in LAI simulations were analyzed to assess the EnKF performance. The DS had superior performance in the calibration and evaluation step with EF = 0.907, 0.878, 0.458 for stalk dry mass, stalk fresh yield (SFY), and LAI, while WO showed EF = 0.622, 0.610, 0.417 for the same variables, respectively. The calibration step affected the OP plot simulation, with DS having higher accuracy (RMSE = 31.678 Mg ha^{-1}) and precision (R^2 = 0.509), compared with WO (RMSE = 39.593 Mg ha^{-1}; R^2 = 0.458). However, after DA, both PBM presented error inconsistency with EnKF, despite the decrease in RMSE (-44.73% and −29.58%) and increase in R^2 (22.15% and 36.50%) of DS and WO, respectively. The error inconsistency diverged from each PBM: the OP simulation of DS overestimated the Landsat LAI; after DA, simulated LAI decreased resulting in SFY underestimation (Bias = -11.469 Mg ha^{-1}); WO showed OP simulations for LAI closer to Landsat's LAI values, despite the positive Bias in SFY estimation, and so EnKF slightly reduced the SFY overestimation (Bias = 22.944 Mg ha^{-1}). Thus, the better descriptions of DS in terms of structure did not inhibit the error inconsistency. We suggested that new studies are required to understand how the assimilated variables impact on the other state variables of the PBM.

1. Introduction

Process-based crop models (PBM) have been largely used for decision making and planning in agriculture, because of the capability of describing how the agricultural system responds to environmental conditions (Morell et al., 2016). The PBMs are capable of a variety of tasks, including yield forecasts in response to weather variables and the impacts of management changes. For that, the PBMs works mechanistically and attempts to explain the genotype × environment × management interactions (Wang et al., 2019). These models consist of organized algorithms that describe physical and biological processes that occur in crop growth and development, and so mimic the interactions among soil, plant, and atmosphere components (Jones et al., 2017). Studies with PBMs are important for advancing the scientific knowledge on crop ecophysiology and management and, when applied as a decision tool, might be able to support government and private agencies, food security policies, and planning (Curnel et al., 2011).

Sugarcane is a key crop because it represents a major world source of sugar and ethanol. Brazil has ca. 8.6 million ha planted with sugarcane, producing ca. 654 million metric tons (Mt) of harvested stalk fresh yield

* Corresponding author.
E-mail address: Izael.fattori@usp.br (I.M. Fattori).

https://doi.org/10.1016/j.compag.2023.107848
Received 21 December 2022; Received in revised form 5 April 2023; Accepted 10 April 2023
Available online 21 April 2023

(CONAB, 2022). Brazil is the world largest producing country, accounting for ca. 38% of global sugarcane production and 50% of global sugar exports (Marin et al., 2019a).

Different PBMs have been developed and evaluated for sugarcane across the world, and these models present different levels of complexity in terms of biophysical process representation in their code (Marin et al., 2015). For example, SAMUCA model (Marin and Jones, 2014; Marin et al., 2017) considers physiological processes such as biomass partitioning at phytomer level, canopy carbon assimilation using leaf assimilation rates, and carboxylation efficiency, and can simulate specific sugarcane traits like plant height, tiller population, sucrose accumulation, and stalk moisture. Furthermore, SAMUCA was recently updated and evaluated considering the effect of the green cane trash blanket effect, arising from management practice in Brazil (Vianna et al., 2020). On the other hand, the WOFOST (WO) (World Food Studies, de Wit et al., 2019) is a more generalist PBM, that can simulate different crops, with a reasonable description of photosynthesis, respiration, biomass portioning, and soil water balance. The WO was adapted for sugarcane simulation (Hu et al., 2019; Scarpare, 2011; van Heemst, 1988), but without simulating specific traits of sugarcane growth and development.

Nevertheless, the mechanist principles of PBMs are only approximations of reality and require a substantial amount of input data and parameters to characterize the soil–plant-atmosphere and the management system, which are sometimes difficult to provide and may vary within the spatial and temporal domains (Manivasagam and Rozenstein, 2020; Marin et al., 2017). One way to reduce the uncertainty of PBM simulations is to insert real-time information by using a data assimilation algorithm (DA) (Huang et al., 2019). These DA methods can be classified into two groups: 1) the variational algorithms, which use all observations of a timestamp to update the model trajectory; 2) the sequential algorithms, which use only the corresponding time observation to estimate the new model state (Huang et al., 2019; Kang and Özdoğan, 2019). One sequential algorithm that has been widely used is the Ensemble Kalman Filter (EnKF) for crop yield estimation (Evensen, 2003; Ines et al., 2013; Pan et al., 2019). The EnKF was tested and outperformed other DA methods for sugarcane simulations using DSSAT/SAMUCA and WOFOST (Fattori Junior et al., 2022; Hu et al., 2019). Because EnKF is capable of counting with both model and observation error, due to the Bayesian approach and a Monte-Carlo realization of the PBM to estimate model error covariance (Wu et al., 2021). Thus, EnKF method assumes the model and observation errors had random white noise, with zero means (Ines et al., 2013).

However, due to the difficulties in model mechanists and the PBM parameterization, the application of PBM frequently includes the Bias (Yo – Ye) (Kang and Özdoğan, 2019), which neglects the assumptions of EnkF that can lead to systematic errors. One example of this is the error inconsistency between leaf area index (LAI) and yield, which happens when PBM simulates LAI values higher than the assimilated, and the open-loop (OP) simulated yield has negative Bias for yield. In these cases, after DA, it is likely that simulations would result in even higher yield underestimation due to the further LAI reduction (Kang and Özdoğan, 2019). That was partly demonstrated by Nearing et al. (2012), who showed that EnKF did not improve wheat yield estimation because of the low correlation between assimilated LAI and crop yield. The absence of prior PBM calibration can also result in error inconsistency, because the use of a set of cultivar-specific parameters cannot describe specific traits of other cultivars, such as higher potential yield and canopy properties (Fattori Junior et al., 2022; Kang and Özdoğan, 2019; Huang et al., 2021). Moreover, model errors related to crop phenology generally resulted in lower accuracy for yield estimation with EnKF, because PBM with more general structures usually account for phenology phase to calculate crop development (e.g. biomass partitioning). In this regard, considering the LAI assimilation, the error in phenology might lead to inconsistency in the magnitude and the peak of the simulated and observed LAI (Curnel et al., 2011; Kang and Özdoğan, 2019).

In contrast, several studies showed improvements in yield estimation after DA. For instance, Yu et al. (2020) used a variant of the EnKF, the Ensemble Smoother, to assimilate sugarcane plant height with an adapted version of WO, finding an expressive improvement for both LAI and yield estimations. Moreover, Fattori Junior et al. (2022) used the EnKF to assimilate LAI with DSSAT/SAMUCA (DS), finding a reasonable improvement in yield estimation compared to the OP simulation. Part of the improvement was due to a more detailed description of plant physiology and soil water process within the model, which can benefit the simulation with the EnKF (Ines et al., 2013). Yet, such benefit was also related to the accuracy of the model without DA, demonstrating that models with high accuracy before DA usually improves the performance gain due to EnKF (Fattori Junior et al., 2022; Kang and Özdoğan, 2019). Moreover, due to a more detailed description of the plant development and growth, it is possible to update variables related to the assimilated variable (e.g. LAI, leaf weight and specific leaf area), and this might reduce the sensitivity of EnKF to model Bias (Ines et al., 2013; Kang and Özdoğan, 2019).

In this regard, Silvestro et al. (2017) compared two different PBMs [Aquacrop and Simple Algorithm for Yield (SAFY)] by assimilating LAI and canopy cover fraction for estimating wheat yield. They found the Aquacrop showing lower accuracy after DA due to a more detailed description of the crop physiology related to water stress. This, in turn, increased the difficulty of the model calibration, due to the larger number of parameters compared to SAFY. However, for each PBM, a different DA method was used, and so the results were not exclusively influenced by the different PBM structures. Therefore, it is still not clear how a more detailed description of the crop development could improve PBM simulation with DA methods and reduce the error inconsistency with EnKF.

To our knowledge, this is the first study to investigate how the PBM structure affected the performance of EnKF. We then aimed to assimilate sugarcane LAI data in two types of PBMs with structures highly different in terms of crop processes descriptions for estimating stalk fresh yield (SFY) and to analyze how those processes and the prior calibration level affected the DA methods performance. To fill this knowledge gap, we calibrated both models with a robust experimental database collected across several producing regions of Brazil and developed a framework to assimilate LAI retrieved from Landsat 7 ETM + and 8/OLI into DS and WO models. We then used the EnKF and tested this framework using a large on-farm sugarmill dataset collected in the most important sugarcane producing region of Brazil. Moreover, we compared the PBMs in terms of their structures involved in the LAI calculation to understand the impact on DA performance.

2. Material and methods

2.1. Data for calibration & evaluation of OP simulations in controlled field experiments

In total, we used a dataset of 13 experiments conducted in a diversity of environments and used the cultivar RB867515, for calibrating (experiments 1–7) and evaluating (experiments 8–13) the PBMs (Table 1). All the experiments received adequate N, P, and K fertilization and regular weed and pest control and were planted using healthy cuttings with 13–15 buds m^{-2}. Row spacing varied from 1.4 m to 1.5 m. Experiments 1–7 had tiller population (TILL), stalk height (SH), LAI, SFY, stalk dry mass (SDM), and sucrose content on a fresh cane basis (POL) obtained by regular sampling. Experiments 8–13, had at last two of these variables sampling during the crop season. A full description of these experiments can be found in Marin et al. (2015) and Vianna et al., (2020).

Soil characteristics and management practices such as planting and harvesting dates, row spacing, mulch cover, and irrigation applications (mm d^{-1}) on each site were prescribed to the model as input

Table 1
Description of experimental datasets used for model calibration and evaluation.

Experiment Number	Location	Planting date	Harvest date	Planting Type	Weather†	Soil‡	Water treatment	Reference
1	Piracicaba/SP 22°41′ S, 47°38′W, 560 m	12/06/2012	10/15/2013	Plant	21.6 °C, 1230 mm, CWa	Typic Hapludox Typic	Irrigated	Vianna et al. (2020)
2		10/15/2013	07/15/2014	1st Ratoon*			Irrigated	
3		10/15/2013	07/15/2014	1st Ratoon			Irrigated	
4		07/15/2014	06/08/2015	2nd Ratoon*			Irrigated	
5		07/15/2014	06/08/2015	2nd Ratoon			Irrigated	
6		06/08/2015	06/08/2016	3rd Ratoon*			Irrigated	
7		06/08/2015	06/08/2016	3rd Ratoon			Irrigated	
8	Aparecida do Taboado/MS 20°05S, 51°18′W, 335 m	07/01/2006	09/08/2007	Plant	23.5 °C, 1560 mm, Aw	Typic Hapludox Typic	Rainfed	Marin et al. (2015)
9	Colina/SP 20°25′S, 48°19′W, 590 m	02/10/2004	06/15/2005	Plant	22.8 °C, 1363 mm, Cwa	Typic Hapludox Typic	Rainfed	
10	Olimpia/SP 20°26′S, 48°32′W, 500 m	02/10/2004	06/15/2005	Plant	23.3 °C, 1349 mm, Cwa	Typic Hapludox Typic	Rainfed	
11	Coruripe/AL 10°07′S, 36°10‘W, 16 *m*	08/16/2005	09/15/2006	Plant	21.6 °C, 1401 mm, As	Fragiudult Typic	Rainfed	
12	União/PI, 4°41′S, 42°52‘W, 68 *m*	03/29/2007	06/16/2008	Plant	27 °C, 1500 mm, Aw	Oxisol	Irrigated	
13	União/PI, 4°41′S, 42°52‘W, 68 m	03/29/2007	06/16/2008	Plant	27 °C, 1500 mm, Aw	Oxisol	Rainfed	

† Respectively: mean annual temperature, annual total rainfall, Koeppen Classification.
‡ U.S. Soil Taxonomy.
* With mulch cover.

information. Also, for experiments 2, 4, and 6 (Table 1) a total of 12 Mg ha^{-1} of green cane straw was considered for simulations. All other experiments were conducted under bare soil conditions. Other details of the experimental data can be found in Table 1.

2.2. Data for data assimilation evaluation

To evaluate the DA with EnKF in our study area, data from 32 plots were collected from a sugarcane mill database located in São Paulo state in Brazil, between the years 2012 to 2015, with an average size of 90,000 m^2. All the plots were managed following the standard for the region and had only the same cultivar RB867515. Each plot was mechanically planted and harvested as a unit and received uniform management and inputs (e.g., fertilizer, pesticides). Only plots with plant-cane were used in this study to reduce the influence of management practices on the crop yield (Marin et al., 2019b, 2021). In that sugarcane mill, plots next to each other were planted and harvested together and then they are usually grouped in blocks in terms of management. We then followed the same approach and grouped the plot data into 7 blocks as described in Table 2. Therefore, all plots of a block had the same planting and harvest date and observed SFY. In this regard, the SFY was simulated for each plot, and to estimate the SFY for each block, the simulated SFY was weighed by area of each plot. The following data were collected from each plot: localization, size, planting date, harvest date, soil classification, and SFY at harvest. The weather data [maximum and minimum air temperature (°C), rainfall (mm), solar radiation (MJ $m^{-2}d^{-1}$) and relative humidity (%)] were collected daily from a weather station installed close to the blocks.

2.3. Satellite image pre-processing

For this study, we used remote sensing data to retrieve LAI as observed data for DA, for real applications with PBM this is the most used source of information. Furthermore, it can provide information during all crop seasons, and reduce the interference of low amounts of data. Thus, the LAI retrieved from Landsat 7 ETM + and 8/OLI were used as observed data to assimilate into WO and DS models. Both sensors had a spatial resolution of 30 m and a revisit frequency of 16-day. The surface reflectance data were obtained by the Google Earth Engine (GEE) (Gorelick et al., 2017), where the images were atmospheric corrected. We used cloud/shadow masks available in eemont, a python package developed by Montero (2021). Also, to eliminate the border effect on plots we applied a buffer on the vector layer to extract pixel values.

The LAI was obtained based on the normalized difference vegetation index (NDVI), calculated with the surface reflectance of Landsat 7 ETM + and 8/OLI, following the relationship proposed by Xavier and Vettorazzi (2004). The relationship between LAI and NDVI was based on

Table 2
Description of block datasets used for data assimilation evaluation.

Blocks	Planting date	Harvest date	Soil Classification¥	Number of plots
1	07/15/2012	12/05/2013	Argissolo Vermelho (Ultisol)	5
2	08/15/2013	09/13/2014	Latossolo Vermelho (Typic Hapludox)	4
3	08/15/2013	09/07/2014	Latossolo Vermelho (Typic Hapludox)	6
4	08/15/2013	09/13/2014	Latossolo Vermelho (Typic Hapludox)	2
5	08/15/2013	09/18/2014	Latossolo Vermelho (Typic Hapludox)	5
6	09/15/2014	07/24/2015	Argissolo Vermelho (Ultisol)	1
7	09/15/2014	12/05/2015	Latossolo Vermelho (Typic Hapludox)	9

¥Soil Classification by Brazilian Soil Classification System (Embrapa, 1999) and their nearest U.S. Soil Taxonomy equivalent (in brackets).

different surface vegetations, but 68% of the data were from sugarcane vegetated surfaces. Thus, for different months of the year, a different equation was obtained (January, March, August, November), being all significant at 1% level ($p < 0.01$), R^2 ranging between 0.54 and 0.74, and the standard error between 0.38 and 0.67. Therefore, for each plot, during the growing season (plant to harvest), an NDVI time series was obtained. Also, the NDVI time series were filtered by the Saviky-Golay method, to reduce the noise caused by the sensor error and atmospheric perturbation (Kang and Özdoğan, 2019; Zhao et al., 2013), after that, the LAI time series were calculated for each plot. The LAI time series was used to represent the observation for the DA with EnKF. Based on the results of Xavier and Vettorazzi (2004) and Abebe et al., (2022a) for the LAI retrieved from remote sensing we considered an error of 30%, for DA with EnKF.

2.4. Brief description of DSSAT/SAMUCA

The SAMUCA model is a PBM firstly developed by Marin and Jones (2014), which is capable to simulate the growth and development of sugarcane crop, implementing an algorithm to describe processes related to phenology, canopy development, tillering, biomass accumulation, root growth, and water stress (Marin et al., 2017). Vianna et al. (2020) improved the SAMUCA model by including recent scientific findings on sugarcane growth at phytomer level, canopy assimilation, and tillering. In this new version, the model was adapted to operate the one-dimensional "tipping bucket" soil water balance and to incorporate the soil temperature to account for the trash blanket effect on sugarcane growth and water use. This presented a superior performance compared with the previous version and was comparable to other widely used PBMs for sugarcane. For this study, we used the SAMUCA model incorporated into the Decision Support System for Agrotechnology Transfer (DSSAT) platform version 4.8 (Jones et al., 2003; Hoogenboom et al., 2019; Vianna et al., 2020), namely DSSAT/SAMUCA (DS).

2.5. Brief description of WOFOST

The WOFOST (WO) model was developed by Wageningen University, the Netherlands, and it was used in this study due to its extensive application and evaluation (Abebe et al., 2022a). The WO model is a mechanistic PBM, which simulates crop growth as a function of solar radiation, temperature and crop properties (Wang et al., 2013). The basis of the simulation is the physiological and ecological progress of crops which includes light interception, CO2 assimilation, respiration, transpiration, phenological development, dry matter accumulation, and partitioning to various organs (Ma et al., 2013). Recently, the WO model was incorporated within the Python Crop Simulation Environment (PCSE) (de Wit et al., 2019). In this study, we implemented DA with the WO model using PCSE, parametrized for sugarcane. The WO is not a simplistic crop model such as SAFY, but rather a generalist PBM that can be adapted for different crops. Thus, WO version used here was not able to simulate specific traits of sugarcane, such as tiller population, plant height, sucrose content, and stem moisture, which are important to define the sugarcane yield. We used the parameters collected and calibrated by Scarpare (2011), for a few Brazilian sugarcane cultivars, as standard for our study.

2.6. Calibration process

The models were calibrated for cultivar RB867515 using the experiments (1–7) present in Table 1. The method used for calibration was the Generalized Likelihood Uncertainty Estimation (GLUE). We used the calibration process described by Marin et al. (2011), Li et al. (2018) and Pereira et al. (2021), following the following steps: (i) Develop prior parameter distributions; in this case, we assume a uniform distribution from a predefined range of variation of genotype parameters, as recommended by Marin et al. (2017), selecting the most sensitive parameters based on Pereira et al. (2021) for DS and Scarpare (2011) for WO (Appendix B - Table 1); (ii) Generate a random set of parameters values from prior parameter distributions based on the Monte Carlo method; for this study we used a sample of 3000 set of parameters; (iii) Run the model with different parameters sets; (iv) The calculus of each likelihood values for each observation (O) was used along with the corresponding simulated outputs to compute the likelihood values, $L(\theta_i|O)$, for each of the N generated parameter vector θ_i following Eq. 1:

$$L(\theta_i|O) = \prod_{J=1}^{M} \frac{1}{\sqrt{2\pi\sigma_o^2}} \exp\left(-\frac{(O_2 - f(\theta_i))^2}{2\sigma_o^2} \right), \text{(i = 1, 2, 3,... N)} \quad (1)$$

$$L_{comb}(\theta_i) = \prod_{k=1}^{K} L_k(\theta_i|O_k) \quad (2)$$

where M is the number of observations replicates; $f(\theta_i)$ is the model output referring to θ_i; σ_o^2 is the variance model errors; K is the number of observations type; $L_{comb}(\theta_i)$ is the combined likelihood value of ith parameter set θ_i. Then, the probability $p(\theta_i)$ of each parameter set was computed with the following Eq. (3):

$$p(\theta_i) = \frac{L(\theta_i|Y)}{\sum_{i=1}^{N} L(\theta_i|Y)} \quad (3)$$

(v) Construct posterior distribution and statistics. The pairs of parameters set and probabilities, $(\theta_i, p_i),\ i = 1, \cdots N,$ were used to construct empirical posterior distributions and to compute the means and variance of selected parameters using the following equations:

$$\widehat{\mu}(\theta) = \sum_{i=1}^{N} p(\theta_i)\,\theta_i \quad (4)$$

$$\widehat{\sigma}(\theta) = \sum_{i=1}^{N} p(\theta_i)(\theta_i - \widehat{\mu})^2 \quad (5)$$

where $\widehat{\mu}(\theta)$ and $\widehat{\sigma}(\theta)$ are the mean and the variance of the posterior distribution, thus, $\widehat{\mu}(\theta)$ is the optimum set of parameters and was considered the calibrated genotype set of parameters and was used in the evaluation step.

The measured data, during the crop season, collected between the experiments in Table 1 were SDM, SFY, LAI, SH, TILL, and POL. For DS all variables were used for performing the GLUE, for the WO model, we only used the SDM, SFY and LAI to calibrate the model, because the WO cannot simulate the other variables. The parameters result in the calibration step were present in Table S1.

2.7. Description of data assimilation procedure

The sequential DA method, EnKF, was used in this study to assimilate LAI derived from Landsat 7 ETM + and 8/OLI. To evaluate the improvements of the EnKF in the model's simulations, the results were compared to the simulation without DA, called open-loop (OP). The EnKF algorithm is described below. To implement the EnKF with DS, the model was adapted to read an input file with a new estimated vector of state variables at any time. Yet, when new LAI values were assimilated by DS, the leaf area and dry weight were also updated at phytomer and block level to ensure the consistency of canopy representation. The version of WOFOST used in this study, inserted in PCSE, is more flexible to be adapted with EnKF. As follows, the simulations can be paused at any time and update the new state variable. For both models, a Python script was developed to read a control file, with each block description, create the input file for model simulation, run the model and pause any time to perform the EnKF and estimate the new LAI values, and finally reinitialize the model and read the outputs. The WO model cannot simulate the SFY, and so we used the relation between SDM and SFY available in the experiments showed in Table 1 to transform the simulated SDM in SFY during the crop cycle (Fig. 1).

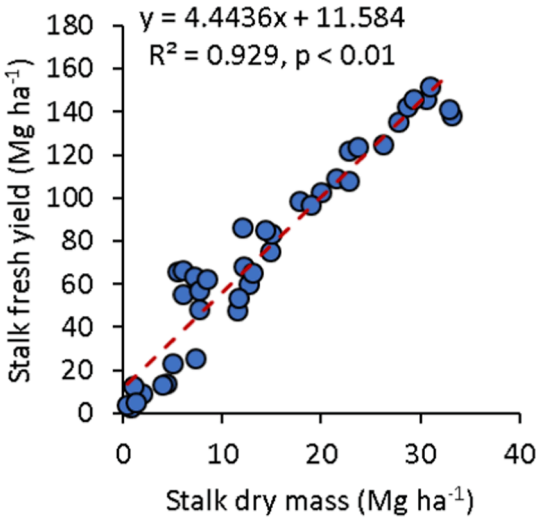

Fig. 1. The relationship between sugarcane stalk fresh yield and corresponding stalk dry mass of experiments in Table 1.

2.8. Ensemble Kalman filter method

The EnKF employs an analytic solution based on two related sources of information, in this case: PBMs outputs and plot observations. These are synthesized to provide a better estimation, with lower variance. For that, the EnKF assumes that the observed data can be related to the state variable xt (LAI in the case of this study) at time t as shown in Eq. (6):

$$y = Hx_t + \varepsilon \tag{6}$$

where y is the observations vector; H is the observation operator that relates to y; ε is a Gaussian random error vector with a mean of zero and observation error covariance R. Also, the forecast of x_t at t = k is Gaussian with mean $x^f_{t=k}$ and error covariance $P^f_{t=k}$. Under these assumptions, the estimated state and error covariance (P) are updated as:

$$x^a_{t=k} = x^f_{t-k} + K\left(y_{t=k} - Hx^f_{t=k}\right) \tag{7}$$

$$P^a_{t=k} = (I - KH)P^f_{t=k} \tag{8}$$

where t is the time index; k is the time of the observed data; f represents the prior state (called forecast) and a is the posterior state (called analysis); I is the identity matrix and K represents the Kalman gain calculated by Eq. (9):

$$K = P^f_{t=k}H^T\left(HP^f_{t=k}H^T + R_{t=k}\right)^{-1} \tag{9}$$

The EnKF forecast and analysis error covariance P^f come directly from an ensemble of the model simulations:

$$P^f H^T = (N_e - 1)^{-1}\sum_{n=1}^{Ne}\left(x^f_n - \overline{x}^f\right)\left(Hx^f_n - H\overline{x}^f\right)^T \tag{10}$$

where Ne is the number of ensemble members, n is a running index for an ensemble member, and $\overline{x}^f$ are the ensemble mean calculated as:

$$\overline{x}^f = N_e^{-1}\sum_{n=1}^{Ne}x^f_n \tag{11}$$

In our study, we only used the LAI retrieved remote sensing as a state variable for DA methods. Thus, H can be taken as an identity matrix (H = 1), with that we can rewrite Eqs. (7), (9), and (10) as Eqs. (12), (13) and (14).

$$x^a_{t=k} = x^f_{t=k} + K\left(y_{t=k} - x^f_{t=k}\right) \tag{14}$$

$$K = P^f_{t=k}\left(P^f_{t=k} + R_{t=k}\right)^{-1} \tag{15}$$

$$P^f = (N_e - 1)^{-1}\sum_{n=1}^{N_e}\left(x^f_n - \overline{x}^f\right)\left(x^f_n - \overline{x}^f\right)^T \tag{16}$$

In EnKF, the observed data were perturbed with the Monte Carlo approach to generate an ensemble, based on the data uncertainty represented by the variance. Because, the observations needed to be treated as random variables and it is commonly assumed that observation errors have a Gaussian distribution (Zhuo et al., 2019). The PBM uncertainties are accounted for by the model ensemble. There are two methods to generate the ensemble members (Zhuo et al., 2019): the first method adds a Gaussian perturbation to the PBM state variables output. The second, add a Gaussian perturbation to the model input parameters. In this study, we used the second method to generate the ensemble members. Thus, to select the most sensitive parameters to LAI, for the DS we used the parameters selected by Fattori Junior et al. (2022), which were MAXGL (maximum number of green leaves a tiller can hold), MLA (maximum leaf area), PLASTOCHRON (thermal time required for the appearance of one new phytomer), INIT_LF_AREA (initial leaf area of first appeared leaf), and MID_TT_LF_GRO (thermal time where leaves can achieve half of its maximum biomass). For the WO we used the parameters that show higher influence in LAI, as reported by Hu et al. (2019) and Scarpare (2011). The parameters selected were TSUMEA (temperature from emergence to anthesis), RGRLAI (maximum relative increase in LAI), TBASE (lower threshold temperature for aging of leaves), EFF (light-use efficiency for real leaf) and CVL (efficiency of conversion into leaves). These parameters were then perturbed to generate an ensemble (40 members), with a gaussian distribution and an uncertainty level of 10% before the simulation started, as recommended by Ines et al. (2013) and Curnel et al. (2011) to optimize the time of the simulation and model accuracy.

After generating the set of parameters, DS runs until the first observed LAI is available. At this point, we calculated in sequence K and the vector $x^a_{t=k}$ (Eqs. (14) and (15), that was considered the optimal estimation of LAI. This step also included a small inflation of 1.5 for LAI in ensemble members, in the case of their variability becoming too low (Ines et al., 2013). This step ensured that the observations were not systematically rejected during assimilation. After that, the estimated LAI is stored in an input file for the next simulations, and runs were re-initialized until the next observations became available.

2.9. Data analysis

The performance of the calibration step was evaluated using the following statistical indices: root mean squared error (RMSE), determination index (R^2), Nash-Sutcliff model efficiency (EF), model Bias (Bias) and Willmot accuracy index (d) (Willmott et al., 2012). Secondly, for the evaluation step with sugarmill plots, we only compared the SFY at the end of the cycle, simulated and observed. Thus, we used the RMSE, R^2 and Bias to compare simulations and observations at block level, for the two models and two methods (OP and EnKF).

3. Results

3.1. Calibration results

Considering the experiments used for calibration (Table 3), the DS outperformed WO, simulating SDM, SFY, and LAI, with an EF = 0.907, 0.878, and 0.458 for DS and 0.622, 0.610 and 0.417 for WO, respectively (Table 3). The accuracy of DS was higher than WO for SDM, SFY, and LAI; Regarding the LAI, WO had RMSE = 0.981 $m^2\ m^{-2}$ and DS, RMSE = 0.946 $m^2\ m^{-2}$. For SDM and SFY, WO had RMSE = 6.442 and 30.349 Mg ha^{-1} and, for DS, RMSE = 3.198 and 16.964 Mg ha^{-1} (Table 3). Furthermore, WO had good precision and accuracy for simulating SDM and SFY, with $R^2 > 0.87$ and $d > 0.90$; LAI presented a lower precision and accuracy with $R^2 = 0.535$ and $d = 0.850$ (Table 3).

Table 3
Statistical indexes of performance of the DSSAT/SAMUCA and WOFOST models in simulating sugarcane crop components across experiments.

Model	Type	Variables	Bias	RMSE	EF	R^2	d	X	Y
DSSAT/SAMUCA	Calibration	SDM	−1.313	3.198	0.907	0.926	0.974	12.587	11.274
		SFY	−9.837	16.964	0.878	0.932	0.964	69.267	59.43
		LAI	−0.456	0.946	0.458	0.645	0.867	3.214	2.759
		POL	0.544	1.262	0.683	0.761	0.92	8.942	9.485
		SH	−0.331	0.53	0.618	0.925	0.853	1.204	0.873
		TILL	−1.551	3.392	0.545	0.667	0.829	14.544	12.993
	Evaluation	SDM	0.657	4.304	0.903	0.951	0.98	19.443	20.1
		SFY	2.675	22.284	0.843	0.915	0.968	84.907	87.582
		LAI	−0.101	0.607	0.583	0.635	0.887	2.595	2.494
		POL	−0.533	1.144	0.547	0.733	0.901	13.232	12.699
		SH	−1.608	3.585	0.517	0.666	0.812	14.03	12.422
		TILL	0.43	0.495	0.673	0.924	0.925	0.963	1.393
WOFOST	Calibration	SDM	5.358	6.442	0.622	0.887	0.911	12.587	17.944
		SFY	24.845	30.349	0.61	0.872	0.903	69.267	94.112
		LAI	−0.157	0.981	0.417	0.535	0.85	3.214	3.058
	Evaluation	SDM	−0.034	4.399	0.899	0.899	0.972	19.443	19.409
		SFY	12.736	24.416	0.811	0.871	0.953	84.907	97.642
		LAI	−0.818	1.243	−0.749	0.252	0.641	2.595	1.777

RMSE: Root mean squared error; EF: Modeling efficiency; R2: Determination index; d: accuracy index of Wilmot; X: Mean observations; Y: Mean simulations; Bias = Y – X; SDM: Stalk dry mass (Mg ha^{-1}); SFY: Stalk fresh yield (Mg ha^{-1}); LAI: Leaf area index (m^2 m^{-2}); POL: sucrose content on a fresh cane basis (% [fresh]); SH: Stalk height (m); TILL: Tiller population (# m^{-2}).

DS had similar performance results, with SDM and SFY showing $R^2 > 0.92$ and $d > 0.96$, as well as for LAI, with $R^2 = 0.645$ and $d = 0.867$ (Table 3). The DS underestimated SDM, SFY, and LAI, with Bias = -1.313 Mg ha^{-1}, −9.837 Mg ha^{-1}, and −0.456 m^2 m^{-2}, respectively, while WO had positive Bias for SDM and SFY (5.358 Mg ha^{-1}, 24.845 Mg ha^{-1}), and negative for LAI (-0.157 m^2 m^{-2}) (Table 3).

The sucrose content in the stalk (POL) is a variable only simulated by DS, for which the model had an acceptable precision ($R^2 = 0.767$; $d = 0.920$; $EF = 0.638$) and accuracy (RMSE = 1.262 %[fresh]) (Table 3). The SH had a higher precision compared to LAI and TILL ($R^2 = 0.925$; $d = 0.853$; $EF = 0.618$) and had RMSE = 0.530 m (Table 3). The TILL had lower performance compared to other variables, except for LAI ($R^2 = 0.667$; $d = 0.829$; $EF = 0.545$; RMSE = 3.392 # m^{-2}) (Table 3). The SH and TILL presented a negative Bias (-0.331 m; −1.551 # m^{-2}) and POL was the only variable in the calibration step that had a positive Bias (0.544 %[fresh]) (Table 3).

The WO presented a lower accuracy for the experiments used for evaluation with RMSE = 4.399 Mg ha^{-1}, 24.416 Mg ha^{-1}, 1.243 m^2 m^{-2}, respectively for SDM, SFY and LAI when compared to DS (RMSE = 4.304, 22.284 Mg ha^{-1}, 0.607 m^2 m^{-2}). Different from the results on calibration step, WO had a negative Bias for SDM (Bias = -0.034 Mg ha^{-1}), and DS positive for SDM and SFY (Bias = 0.657, 2.675 Mg ha^{-1}). Yet, both models had negative Bias for LAI, being −0.101 m^2 m^{-2} and −0.818 m^2 m^{-2} respectively for DS and WO (Table 3). The WO showed lower performance for simulating LAI (EF = -0.749, $R^2 = 0.252$, $d = 0.641$), but it was satisfactory for SDM and SFY ($EF > 0.81$, $R^2 > 0.87$, $d > 0.95$) (Table 3). The DS had good performance for simulating SDM and SFY ($EF > 0.84$, $R^2 > 0.91$, $d > 0.96$), although lower for LAI ($EF = 0.583$, $R^2 = 0.635$, $d = 0.887$) (Table 3).

3.2. Data assimilation evaluation

The DS OP simulations had a higher accuracy for final SFY (RMSE = 31.678 Mg ha^{-1}) compared to WO (RMSE = 39.593 Mg ha^{-1}) and higher precision ($R^2 = 0.509$ and 0.458 for DS and WO, respectively) (Table 4). Both models had a positive Bias for OP simulations, 25.406 Mg ha^{-1} for DS and 31.282 Mg ha^{-1} for WO (Table 4).

When DA based on EnKF using LAI was performed, the DS had RMSE = 17.508 Mg ha^{-1}, which represented a decrease of −44.73 % compared to the OP method (Table 4). The WO had lower accuracy compared to DS (RMSE = 27.880 Mg ha^{-1}), and it represented a decrease of −29.58% compared with OP methods (Table 4). The precision also improved after DA, as DS showed $R^2 = 0.622$, an increase of 22.15% compared to OP.

Table 4
Statistical indexes of performance of DSSAT/SAMUCA and WOFOST without data assimilation, open-loop method (OP), and with data assimilation using the Ensemble Kalman Filter (EnKF).

Model	Method	Bias	RMSE	R^2	X	Y
DSSAT/SAMUCA	OP	25.406	31.678	0.509*	94.701	120.107
	EnKF	−11.469	17.508	0.622*	94.701	83.232
WOFOST	OP	31.282	39.593	0.458*	94.701	125.983
	EnKF	22.944	27.880	0.625*	94.701	117.645

RMSE: Root mean squared error; R^2: Determination index; X: Mean observations; Y: Mean simulations; Bias = Y - X.
*$p < 0.01$.

The WO had an even higher increase in precision (36.50%), with $R^2 = 0.625$, which was higher than DS (Table 4). The DS with EnKF had Bias = -11.469 Mg ha^{-1}, while WO showed a positive Bias = 22.944 Mg ha^{-1} after DA with EnKF (Table 4).

After DA, DS simulated lower values of SFY, with mean = 83.232 Mg ha^{-1}, compared to SFY simulated by WO (mean = 117.645 Mg ha^{-1}, Table 4). Further, after DA, DS had some blocks with SFY simulated lower than the values observed, different from WO, that had a lower accuracy reduction and any SFY simulated lower than observed ones (Fig. 2). In this regard, the WO improved the simulations of 5 blocks out of 8, while DS improved 4 blocks out of 8. For WO, however, the blocks without improvements in accuracy were those that already had high accuracy before DA. (Fig. 2).

During the crop cycle, the DS showed higher LAI values for OP simulations compared to WOFOST and Landsat LAI, in general for all plots, as shown for two selected plots in Fig. 3. Higher differences between DS and Landsat LAI were observed in the early phases of crop development when the LAI increases following a linear relationship (Fig. 3 a and i). The LAI simulated by DS had a peak in the early stage of development and, after that, LAI decreased and stabilized at a lower level. This was different from what Landsat LAI showed, for which the peak period occurred at later stages of development (Fig. 3 a and i). For WO, LAI profiles also had a peak period in an earlier stage compared to Landsat LAI, but the values were closer to the observed ones along the crop season (Fig. 3 c and k).

Therefore, two types of error inconsistency occurred in the simulations, for each PBM. For DS, first, the plots with lower SFY, simulated by OP, (Fig. 3 m) had LAI values higher than the Landsat LAI (Fig. 3 j).

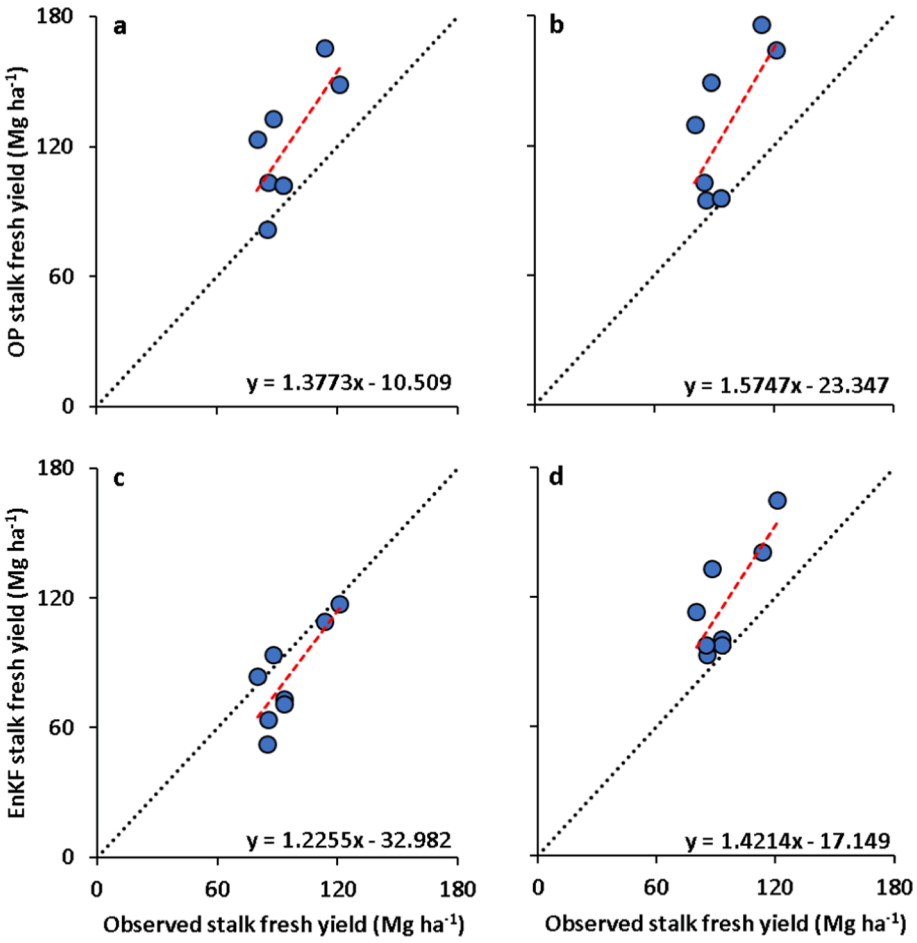

Fig. 2. Comparison of observed and simulated stalk fresh yield (SFY) (a, b) with open-loop simulations (OP) and (c, d) with Ensemble Kalman filter (EnKF), using (a, c) DSSAT/SAMUCA and (b, d) WOFOST. The dashed black line represents the 1:1 adjustment, whereas the red dashed line is the regression between observed SFY and simulated SFY. The statistical indexes of the plots can be found in Table 4. (For interpretation of the references to colour in this figure legend, the reader is referred to the web version of this article.)

However, the OP simulations resulted in SFY lower than the observed (Fig. 3 m). Thus, after DA, the negative Bias for SFY was even increased (Fig. 3 n). Second, a mismatch between the LAI's peak period was observed for all plots (Fig. 3 a and i), which mainly reduced the performance of LAI assimilated in blocks with low SFY (Fig. 3 j and n). For WO, the OP simulated LAI was closer to the Landsat LAI (Fig. 3 c and k), but SFY had positive Bias mainly for plots with high observed SFY (Fig. 3 g). Thus, after DA, the high Bias in SFY was slightly lowered (Fig. 3 h). Moreover, the WO simulations had a mismatch between OP LAI and Landsat LAI, with higher values in the early development phases and lower at the end of the crop cycle, mainly for plots with higher SFY simulations (Fig. 3 c and k).

Nevertheless, WO after DA showed higher accuracy for the plots with lower observed SFY, because the simulated LAI had better agreement with the Landsat LAI, and closer SFY simulated values with observed ones (Fig. 3 l and p). For DS, the simulations after DA had higher accuracy for block with high SFY (Fig. 3 e and f).

The higher decrease in DS SFY estimation followed a higher decrease in LAI values, after DA, along crop cycle, compared to WO (Fig. 3). In summary, the OP simulations of LAI presented a mean value (1.347 m^2 m^{-2}), which was close to the Landsat LAI (1.350 m^2 m^{-2}), while DS showed mean LAI = 2.485 m^2 m^{-2}, which was 84% higher than mean Landsat LAI (Fig. 4). Thus, despite WO having higher mean SFY OP simulations (125.983 Mg ha^{-1}), the simulated LAI values were lower than DS, which present lower average SFY OP simulations (120.208 Mg ha^{-1}) (Table 4).

4. Discussion

In this study, the models DS and WO were calibrated for cultivar RB867515 and had the SFY simulations, using the EnKF, compared with the same plot database by assimilating LAI retrieved from Landsat 7 ETM + and 8 OLI. In the calibration step, the DS had better performance for calibration and evaluation, despite the higher number of observed variables used for GLUE. Thus, it seems that simulating different plant variables resulted in a lower uncertainty, despite the higher complexity and interactions. For example, SDM is partly derived from the TILL and SH, and adding these relationships to the model and using this observed variable for calibration, we found better simulations for SDM and SFY. Furthermore, these results may also be due to a more detailed description of the soil–water balance and soil layers of DS, which is different from the WO that considers only one soil layer.

One important part of the lower performance of WO came from the ratoon experiments (2–7, Table 1), as the model overestimated the SDM, SFY, and LAI for them. This can be related to some parameters of WO, such as initial total crop dry weight (TDWI); degree-days from emergence to anthesis (TSUM1); and initial rooting depth (RDI), that were not retrieved from these experiments. Therefore, the parameters retrieved from Scarpare (2011) might not represent the conditions of these experiments, because they were derived from different environments and genotypes. Moreover, despite both PBMs having the same database for calibration and the same weather database, the uncertainty in PBM structure and the difference in soil and genotype parameters affected the performance of the simulations (Marin et al., 2015).

The calibration performance affected the sugarmill plots simulations, with DS showing higher performance for OP simulations than WO (Table 3 and 4). However, OP simulations with DS had lower accuracy, compared to the results of Fattori Junior et al. (2022), which use the same PBM for simulating different experiments with EnKF and LAI retrieved from experimental observations. Moreover, comparing the

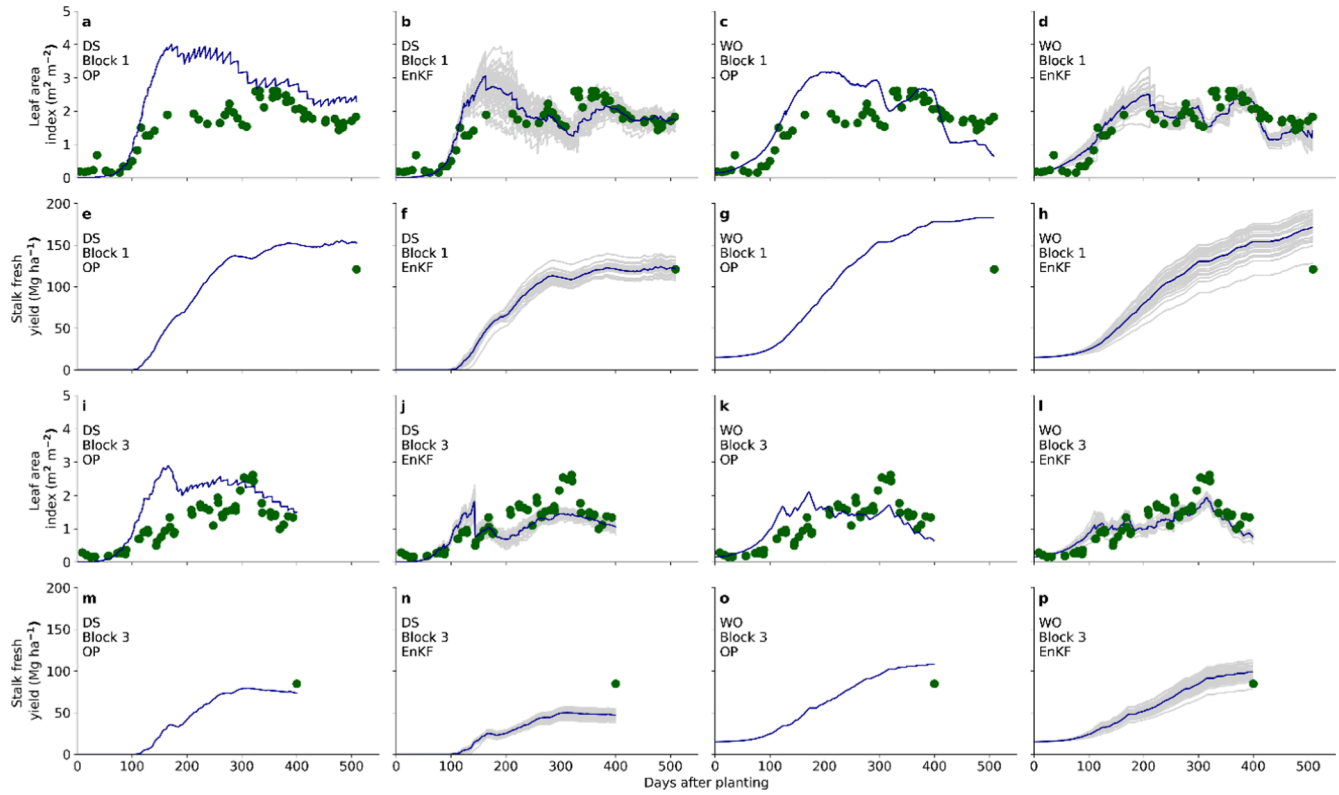

Fig. 3. Comparison between simulated (dark blue lines) and observed (green circles) leaf area index (LAI) retrieved from Landsat and stalk fresh yield (SFY) for one of the plot of block 1 and 3, with open-loop (OP) and Ensemble Kalman filter (EnKF) method, using the DSSAT/SAMUCA (DS) and WOFOST (WO). Greys lines are the ensemble simulations, blue lines are the ensemble mean. (For interpretation of the references to colour in this figure legend, the reader is referred to the web version of this article.)

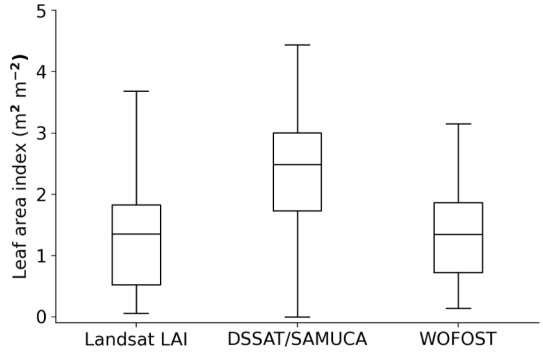

Fig. 4. Box-plot of sugarcane leaf area index (LAI, m^2 m^{-2}) distribution retrieved from Landsat 7 ETM + and 8 OLI, and open-loop simulations with DSSAT/SAMUCA and WOFOST model.

results of WO with other studies, the OP simulations presented lower accuracy, with higher RMSE than studies with the same model (Abebe et al., 2022a; Hu et al., 2019). The lower accuracy of both PBMs can be a result of management adopted in sugarmill plots that were more susceptible to reducing factors (diseases, weeds, pests, soil compaction and failures), which decreased the SFY and were not simulated by the PBMs (Dias and Sentelhas et al., 2017; Gasparotto et al., 2022).

Nevertheless, the use of EnKF reduced the RMSE and increased R^2 for both models (Table 4), showing the potential of using LAI retrieved from Landsat 7 ETM + and 8 OLI for reducing model uncertainty (Abebe et al., 2022a; Huang et al., 2015; Kang and Özdoğan, 2019). It showed, also, the potential for using DA methods to correct the model simulation when reduction factors were present (Hu et al., 2019). Yet, matters to highlight that despite both models having the same assimilated variable and used the same database for calibration, the results after DA were considerably different, which indicates that the PBM structure highly affected the performance of SFY estimation after DA (Silvestro et al., 2017).

In this regard, the light interception mechanics and the distribution over the canopy are similar between both PBMs. Both account for solar radiation being fractionated between direct and diffuse proportions (Vianna et al., 2020; de Wit et al., 2019), and the leaf area is a result of total living leaves and the specific leaf area. Therefore, the difference between models was the mechanism used to calculate the living leaf biomass and the values used for specific leaf area. For DS, the leaf biomass was calculated by phytomer and the total leaf biomass per area was a result of the number of phytomers with living leaves, leaf biomass of each phytomer, and the number of stalks (Vianna et al., 2020). Moreover, the senescence rate of leaves was related to the process of shading leaves, the maximum number of leaves, leaves age, and tiller age, in conditions without water stress. Further, the specific leaf area was considered a fixed parameter during the crop simulation. The WO, in turn, does not simulate the sugarcane number of tillers and phytomers, and the leaf biomass was calculated by leaves age (de Wit et al., 2019), which also affects the calculus of LAI, leaf area, and leaf senescence. The relation between leaf area and stalk mass was only related to partitioning factors, over the crop development stage. Different from DS, the specific leaf area changes during the crop development stages, following the input values.

Therefore, the DS had a more complex structure for LAI simulations, which was affected by the number of stalks and phytomers, which represent a better approximation of the sugarcane development (Lou et al., 2013; Zhou and Shoko, 2011). This mechanism might explain part of the better accuracy and precision of DS for calibration and evaluation steps (Table 3), because enough information (LAI and TIL) was provided for calibration (Vianna et al., 2020). This also may explain part of the

better performance of DS in OP simulations, for the sugarmill blocks simulations (Table 4).

Furthermore, the ensemble state used to describe the possibility of real states in crop growth simulations also influenced on DA performance. Both models had five parameters perturbed to generate the initial ensemble, however, these parameters diverged from each model, which led to a large difference in the background error, and then influencing the performance of EnKF. The DS parameters perturbed were tightly linked to LAI, differently from WO, which had two of the five parameters more generalist (EFF and TSUMEA). However, background error generated by the DS parameters could not inhibit filter divergences. For block 3, the DS model showed filter divergences after assimilating several low values of remote sensed LAI, between 300 and 400 days after planting (Fig. 3j). Since the model errors became lower, the assimilation higher LAI values made low contribution to the LAI analysis, leading to an LAI and SFY underestimation. For WO in the same period, the DA resulted in LAI values close to the remote sensed LAI (Fig. 3i), showing that background error was higher than DS. Yet, such filter divergence was also influenced by the higher errors in Landsat LAI.

The DA performance had a close relationship with the OP performance (Fattori Junior et al., 2022), and after DA, the DS had also higher accuracy compared to WO. However, the DS underestimated the SFY (Table 4), because the changes in LAI values after DA had a direct relationship with SFY simulation. In this regard, when OP simulations had LAI and yield (SFY) both with positive Bias, but the Bias in SFY was slightly lower, after DA the SFY significantly reduced, resulting in large errors (Kang and Özdoğan, 2019). However, when both LAI and SFY had high Bias, after DA, the accuracy was notably improved. For WO, the resulted LAI from OP and the Landsat LAI had close values, thus when the model had high positive Bias for SFY estimation, the SFY after DA was only slightly improved (Kang and Özdoğan, 2019); however, the Bias for LAI was close to zero, the DA was not able to improve the SFY estimations.

Therefore, our results emphasize that the structure of DS and WO could not reduce the sensitivity of EnKF of both PBM and assimilated variable Bias. This disagrees with the hypothesis that updating state variables related to LAI reduces the sensitivity of EnKF to model Bias (Ines et al., 2013; Kang and Özdoğan, 2019). The target variable to be improved was the SFY, but the variable assimilated was LAI, and between LAI and SFY there are several complex relationships affected by many other factors (Nearing et al., 2012). Also, the LAI of sugarcane has a considerable variation among genotype and environment (Lou et al., 2013; Marin et al., 2011), which reflects in the relationship between LAI and other variables important to define the SFY, such as SH and TILL (Yu et al., 2020; Zhou and Shoko, 2011). Thus, by only assimilating LAI and updating the related variables was not sufficient for inhibiting the error inconsistency. So, the correlation between LAI and variables such as TILL and SH should be better explored and improved when the LAI is assimilated into the PBM. Further, using one or more assimilated variables would reduce the impact of Biased variables (Yu et al., 2022, Pan et al., 2019), and might lower the EnKF sensitivity. Further studies should then explore this considering different model structures.

In terms of practicalities, the WO model was easily coupled with EnKF due to object-oriented construction in Python. Thus, multiple simulations can be initialized and paused at any time during the simulation runs, to perform the DA. Different from the DS, the structure of DSSAT platforms did not allow for a pause in the simulations during the model run. Therefore, to perform the DA, the models need to be reinitialized at each observation, increasing the time of simulations, despite the FORTRAN language being faster. One option to overcome this was found by Ines et al. (2013), who used a modified version of CSM-Maize model outside the DSSAT plataform, thus allowing EnKF to control the simulation ensemble with independent crop model runs to improve the speed and applicability with EnKF.

Although the EnKF techniques employed in this study showed improved performance of SFY simulations for both models, we emphasized some limitations of our study. The LAI time series retrieved from Landsat 7 ETM + and 8/OLI, used the relationship of Xavier and Vettorazzi (2004), which in turn used data from surface vegetation cover that was partly retrieved from other crops and may not well represent the sugarcane LAI. In this regard, during the DA process, we assumed a relatively high LAI error for generating the ensembles, and this may interfere with DA performance.

Therefore, further studies should explore the differences between PBMs with LAI observations retrieved from more sophisticated models such as biophysics models (Pan et al., 2019) and the Gaussian process (Abebe et al., 2022b). Finally, in this study we used the standard version of EnKF, but other studies developed different variations of the EnKF to overcome some limitations of the method (Jamal and Linker, 2020; Wu et al., 2021), and so these can be tested in future researchers to compare the interference in more PBMs.

5. Conclusion

Both evaluated PBM had satisfactory performance in the calibration and evaluation step, but the DS had better performance, as shown by the OP simulations results in terms of accuracy (RMSE) and precision (R^2), compared to WO. The DS had a more detailed process description of the relationship between LAI and other crop related variables in its structure, which improved OP simulations. After DA, both PBMs showed error inconsistency, and both were improved in terms of accuracy and precision. The error inconsistency however diverged from each PBM: the OP simulation of DS overestimated the Landsat LAI; after DA, simulated LAI decreased resulting in SFY underestimation; WO showed OP simulations for LAI closer to Landsat's LAI values, despite the positive Bias in SFY estimation, and so EnKF slightly reduced the SFY overestimation. The EnKF performance was also influenced by the genotype parameters used to generate the ensemble simulations, resulting in different backgrounds error for each model. Thus, the better descriptions of DS in terms of structure did not inhibit the error inconsistency, which contradicts the hypothesis initially raised in the literature. This study emphasized that the relations among LAI and other crop variables should be more deeply considered in the DA process, for a more complete benefit of DA in the quality of simulations.

CRediT authorship contribution statement

Izael M. Fattori: Conceptualization, Methodology, Software, Formal analysis, Writing – original draft, Writing – review & editing. **Fábio R. Marin:** Supervision, Conceptualization, Funding acquisition, Writing – review & editing.

Declaration of Competing Interest

The authors declare that they have no known competing financial interests or personal relationships that could have appeared to influence the work reported in this paper.

Data availability

Data will be made available on request.

Acknowledgements

We thank the São Paulo Research Foundation (FAPESP, grants 2021/00720-0 and 2014/05887-6), Brazilian Research Council (CNPq, 100094/2019-8, 301424/2015-2, 300916/2018-3, 401662/2016-0 and 425174/2018-2).

Appendix A. Supplementary data

Supplementary data to this article can be found online at https://doi.

org/10.1016/j.compag.2023.107848.

References

Abebe, G., Tadesse, T., Gessesse, B., 2022a. Assimilation of leaf Area Index from multisource earth observation data into the WOFOST model for sugarcane yield estimation. Int. J. Remote Sens. 43, 698–720. https://doi.org/10.1080/01431161.2022.2027547.

Abebe, G., Tadesse, T., Gessesse, B., 2022b. Estimating Leaf Area Index and biomass of sugarcane based on Gaussian process regression using Landsat 8 and Sentinel 1A observations. Int. J. Image Data Fusion 00, 1–31. https://doi.org/10.1080/19479832.2022.2055157.

CONAB National Supply Company, 2022 Products and services. https://www.conab.gov.br/info-agro/safras/cana (Accessed 07 February 2022).

Curnel, Y., de Wit, A.J.W., Duveiller, G., Defourny, P., 2011. Potential performances of remotely sensed LAI assimilation in WOFOST model based on an OSS Experiment. Agric. For. Meteorol. 151, 1843–1855. https://doi.org/10.1016/j.agrformet.2011.08.002.

de Wit, A., Boogaard, H., Fumagalli, D., Janssen, S., Knapen, R., van Kraalingen, D., Supit, I., van der Wijngaart, R., van Diepen, K., 2019. 25 years of the WOFOST cropping systems model. Agric. Syst. 168, 154–167. https://doi.org/10.1016/j.agsy.2018.06.018.

Dias, H.B., Sentelhas, P.C., 2017. Evaluation of three sugarcane simulation models and their ensemble for yield estimation in commercially managed fields. F. Crop. Res. 213, 174–185. https://doi.org/10.1016/j.fcr.2017.07.022.

Evensen, G., 2003. The Ensemble Kalman Filter: theoretical formulation and practical implementation. Ocean Dyn. 53, 343–367. https://doi.org/10.1007/s10236-003-0036-9.

Embrapa, 1999. Brazilian Soil Classification System (Abstract in English). EMBRAPA, Rio de Janeiro.

Fattori Junior, I.M., Vianna, M.S., Marin, F.R., 2022. Assimilating leaf area index data into a sugarcane process-based crop model for improving yield estimation. Eur. J. Agron 136, 126501. https://doi.org/10.1016/j.eja.2022.126501.

Gasparotto, L.G., Rosa, J.M., Grassini, P., Marin, F.R., 2022. Developing an operational framework to diagnose yield gaps in commercial sugarcane mills. Field Crops Research 278, 108433. https://doi.org/10.1016/j.fcr.2022.108433.

Gorelick, N., Hancher, M., Dixon, M., Ilyushchenko, S., Thau, D., Moore, R., 2017. Google Earth Engine: planetary-scale geospatial analysis for everyone. Remote Sens. Environ. 202, 18–27. https://doi.org/10.1016/j.rse.2017.06.031.

Hoogenboom, G., Porter, C.H., Boote, K.J., Shelia, V., Wilkens, P.W., Singh, U., White, J.W., Asseng, S., Lizaso, J.I., Moreno, L.P., Pavan, W., Ogoshi, R., Hunt, L.A., Tsuji, G.Y., Jones, J.W., 2019. The DSSAT crop modeling ecosystem. In: Boote, K.J. (Ed.), Advances in Crop Modeling for a Sustainable Agriculture. Burleigh Dodds Science Publishing, Cambridge, United Kingdom, pp. 173–216.

Hu, S., Shi, L., Huang, K., Zha, Y., Hu, X., Ye, H., Yang, Q., 2019. Improvement of sugarcane crop simulation by SWAP-WOFOST model via data assimilation. F. Crop. Res. 232, 49–61. https://doi.org/10.1016/j.fcr.2018.12.009.

Huang, J., Tian, L., Liang, S., Ma, H., Becker-Reshef, I., Huang, Y., Su, W., Zhang, X., Zhu, D., Wu, W., 2015. Improving winter wheat yield estimation by assimilation of the leaf area index from Landsat TM and MODIS data into the WOFOST model. Agric. For. Meteorol. 204, 106–121. https://doi.org/10.1016/j.agrformet.2015.02.001.

Huang, J., Gómez-Dans, J.L., Huang, H., Ma, H., Wu, Q., Lewis, P.E., Liang, S., Chen, Z., Xue, J.H., Wu, Y., Zhao, F., Wang, J., Xie, X., 2019. Assimilation of remote sensing into crop growth models: current status and perspectives. Agric. For. Meteorol. 276–277, 107609 https://doi.org/10.1016/j.agrformet.2019.06.008.

Huang, X., Zhao, G., Zorn, C., Tao, F., Ni, S., Zhang, W., Tu, T., Höglind, M., 2021. Grass modelling in data-limited areas by incorporating MODIS data products. F. Crop. Res. 271, 108250 https://doi.org/10.1016/j.fcr.2021.108250.

Ines, A.V.M., Das, N.N., Hansen, J.W., Njoku, E.G., 2013. Assimilation of remotely sensed soil moisture and vegetation with a crop simulation model for maize yield prediction. Remote Sens. Environ. 138, 149–164. https://doi.org/10.1016/j.rse.2013.07.018.

Jamal, A., Linker, R., 2020. Genetic operator-based particle filter combined with Markov chain monte Carlo for data assimilation in a crop growth model. Agriculture 10 (12), 606. https://doi.org/10.3390/agriculture10120606.

Jones, J.W., Hoogenboom, G., Porter, C., Boote, K., Batchelor, W., Hunt, L., Wilkens, P., Singh, U., Gijsman, A., Ritchie, J., 2003. The DSSAT cropping system model. Eur. J. Agron. 18, 235–265. https://doi.org/10.1016/S1161-0301(02)00107-7.

Jones, J.W., Antle, J.M., Basso, B., Boote, K.J., Conant, R.T., Foster, I., Godfray, H.C.J., Herrero, M., Howitt, R.E., Janssen, S., Keating, B.A., Munoz-Carpena, R., Porter, C.H., Rosenzweig, C., Wheeler, T.R., 2017. Brief history of agricultural systems modeling. Agric. Syst. 155, 240–254. https://doi.org/10.1016/j.agsy.2016.05.014.

Kang, Y., Özdoğan, M., 2019. Field-level crop yield mapping with Landsat using a hierarchical data assimilation approach. Remote Sens. Environ. 228, 144–163. https://doi.org/10.1016/j.rse.2019.04.005.

Li, Z., He, J., Xu, X., Jin, X., Huang, W., Clark, B., Yang, G., Li, Z., 2018. Estimating genetic parameters of DSSAT-CERES model with the GLUE method for winter wheat (Triticum aestivum L.) production. Comput. Electron. Agric. 154, 213–221. https://doi.org/10.1016/j.compag.2018.09.009.

Luo, J., Que, Y., Zhang, H., Xu, L., 2013. Seasonal variation of the canopy structure parameters and its correlation with yield-related traits in sugarcane. Sci. World J. 2013 https://doi.org/10.1155/2013/801486.

Ma, H., Huang, J., Zhu, D., Liu, J., Su, W., Zhang, C., Fan, J., 2013. Estimating regional winter wheat yield by assimilation of time series of HJ-1 CCD NDVI into WOFOST-ACRM model with Ensemble Kalman Filter. Math. Comput. Model. 58, 759–770. https://doi.org/10.1016/j.mcm.2012.12.028.

Manivasagam, V.S., Rozenstein, O., 2020. Practices for upscaling crop simulation models from field scale to large regions. Comput. Electron. Agric. 175 https://doi.org/10.1016/j.compag.2020.105554.

Marin, F.R., Vianna, M.S., Nassif, D.S., 2019a. Challenges, Constraints, and Limitations of Cane Biofuels. In: Sugarcane Biofuels. Springer, Cham, pp. 389–407. 10.1007/978-3-030-18597-8_17.

Marin, F.R., Jones, J.W., Royce, F., Suguitani, C., Donzeli, J.L., Filho, W.J.P., Nassif, D.S., 2011. Parameterization and evaluation of predictions of DSSAT/CANEGRO for Brazilian sugarcane. Agron. J. 103 (2), 304–315. https://doi.org/10.2134/agronj2010.0302.

Marin, F.R., Jones, J.W., 2014. Process-based simple model for simulating sugarcane growth and production. Sci. Agric. 71, 1–16. https://doi.org/10.1590/S0103-90162014000100001.

Marin, F., Jones, J.W., Boote, K.J., 2017. A stochastic method for crop models: including uncertainty in a sugarcane model. Agron. J. 109, 483–495. https://doi.org/10.2134/agronj2016.02.0103.

Marin, F.R., Thorburn, P.J., Nassif, D.S.P., Costa, L.G., 2015. Sugarcane model intercomparison: structural differences and uncertainties under current and potential future climates. Environ. Model. Softw. 72, 372–386. https://doi.org/10.1016/j.envsoft.2015.02.019.

Marin, F.R., Rattalino Edreira, J.I., Andrade, J., Grassini, P., 2019b. On-farm sugarcane yield and yield components as influenced by number of harvests. F. Crop. Res. 240, 134–142. https://doi.org/10.1016/j.fcr.2019.06.011.

Marin, F.R., Rattalino Edreira, J.I., Andrade, J.F., Grassini, P., 2021. Sugarcane yield and yield components as affected by harvest time. Sugar Tech. https://doi.org/10.1007/s12355-020-00945-5.

Montero, D., 2021. eemont: a Python package that extends Google Earth Engine. J. Open Source Softw. 6.

Morell, F.J., Yang, H.S., Cassman, K.G., Wart, J.V., Elmore, R.W., Licht, M., Coulter, J.A., Ciampitti, I.A., Pittelkow, C.M., Brouder, S.M., Thomison, P., Lauer, J., Graham, C., Massey, R., Grassini, P., 2016. Can crop simulation models be used to predict local to regional maize yields and total production in the U.S. Corn Belt? F. Crop. Res. 192, 1–12. https://doi.org/10.1016/j.fcr.2016.04.004.

Nearing, G.S., Crow, W.T., Thorp, K.R., Moran, M.S., Reichle, R.H., Gupta, H.V., 2012. Assimilating remote sensing observations of leaf area index and soil moisture for wheat yield estimates: an observing system simulation experiment. Water Resour. Res. 48, 1–13. https://doi.org/10.1029/2011WR011420.

Pan, H., Chen, Z., de Allard, W., Ren, J., 2019. Joint assimilation of leaf area index and soil moisture from sentinel-1 and sentinel-2 data into the WOFOST model for winter wheat yield estimation. Sensors (Switzerland) 19. https://doi.org/10.3390/s19143161.

Pereira, R.A. de A., Vianna, M. dos S., Nassif, D.S.P., Carvalho, K. dos S., Marin, F.R., 2021. Global sensitivity and uncertainty analysis of a sugarcane model considering the trash blanket effect. Eur. J. Agron. 130, 126371. 10.1016/j.eja.2021.126371.

Scarpare, F.V., 2011. Simulação do crescimento da cana-de-açúcar pelo modelo agrohidrológico SWAP/WOFOST. Universidade de São Paulo, Escola Superior de Agricultura "Luiz de Queiroz". Piracicaba, Brasil (In Portuguese).

Silvestro, P.C., Pignatti, S., Pascucci, S., Yang, H., Li, Z., Yang, G., Huang, W., Casa, R., 2017. Estimating wheat yield in China at the field and district scale from the assimilation of satellite data into the Aquacrop and simple algorithm for yield (SAFY) models. Remote Sens. 9, 1–24. https://doi.org/10.3390/rs9050509.

Van Heemst, H.D.J., 1988. Plant data values required for simple crop growth simulation models: review and bibliography.

Vianna, M. dos S., Nassif, D.S.P., dos Santos Carvalho, K., Marin, F.R., 2020. Modelling the trash blanket effect on sugarcane growth and water use. Comput. Electron. Agric. 172, 105361. 10.1016/j.compag.2020.105361.

Wang, E., Brown, H.E., Rebetzke, G.J., Zhao, Z., Zheng, B., Chapman, S.C., 2019. Improving process-based crop models to better capture genotype×environment×management interactions. J. Exp. Bot. 70, 2389–2401. https://doi.org/10.1093/jxb/erz092.

Wang, J., Li, X., Lu, L., Fang, F., 2013. Parameter sensitivity analysis of crop growth models based on the extended Fourier Amplitude Sensitivity Test method. Environ. Model. Softw. 48, 171–182. https://doi.org/10.1016/j.envsoft.2013.06.007.

Willmott, C.J., Robeson, S.M., Matsuura, K., 2012. A refined index of model performance. Int. J. Climatol. 32 (13), 2088–2094. https://doi.org/10.1002/joc.2419.

Wu, S., Yang, P., Ren, J., Chen, Z., Li, H., 2021. Regional winter wheat yield estimation based on the WOFOST model and a novel VW-4DEnSRF assimilation algorithm. Remote Sens. Environ. 255 https://doi.org/10.1016/j.rse.2020.112276.

Xavier, A.C., Vettorazzi, C.A., 2004. Mapping leaf area index through spectral vegetation indices in a subtropical watershed. Int. J. Remote Sens. 25, 1661–1672. https://doi.org/10.1080/01431160310001620803.

Yu, D., Zha, Y., Shi, L., Jin, X., Hu, S., Yang, Q., Huang, K., Zeng, W., 2020. Improvement of sugarcane yield estimation by assimilating UAV-derived plant height observations. Eur. J. Agron. 121, 126159 https://doi.org/10.1016/j.eja.2020.126159.

Yu, D., Zha, Y., Shi, L., Ye, H., Zhang, Y., 2022. Improving sugarcane growth simulations by integrating multi-source observations into a crop model. Eur. J. Agron. 132, 126410 https://doi.org/10.1016/j.eja.2021.126410.

Zhao, Y., Chen, S., Shen, S., 2013. Assimilating remote sensing information with crop model using Ensemble Kalman Filter for improving LAI monitoring and yield

estimation. Ecol. Modell. 270, 30–42. https://doi.org/10.1016/j.ecolmodel.2013.08.016.

Zhou, M.M., Shoko, M.D., 2011. Seasonal and varietal effects on tiller population development of sugarcane (*Saccharum officinarum* L.). South African J. Plant Soil 28 (1), 11–16.

Zhuo, W., Huang, J., Li, L., Zhang, X., Ma, H., Gao, X., Huang, H., Xu, B., Xiao, X., 2019. Assimilating soil moisture retrieved from Sentinel-1 and Sentinel-2 data into WOFOST model to improve winter wheat yield estimation. Remote Sens. 11, 1618. https://doi.org/10.3390/rs11131618.